Excitation transport and trapping on spectrally disordered lattices

John M. Jean, Chi-Kin Chan, G. R. Fleming, and Thomas G. Owens*
Department of Chemistry and The James Franck Institute, The University of Chicago, Chicago, Illinois 60637; and
*Section of Plant Biology, Cornell University, Ithaca, New York 14853

ABSTRACT It is widely assumed that the decay of fluorescence in photosynthetic systems can be described as a sum of exponential components and that the amplitude of each component is directly related to the absorption cross-section of the antenna pigments coupled to the fluorescing species. We present exact calculations of excited state decay in two-dimensional regular lattices of different geometries containing multiple spectral forms of antenna pigments. We illustrate by these calculations that there is no simple relation between the decay amplitudes (and resulting time-resolved excitation spectra) and the steady-state absorption spectra. Only in the limit that the electronic excitations reach a rapid equilibrium among all antenna spectral forms does the excitation spectrum depend uniquely on the spectral features of the array. Using the simulations in conjunction with our recent fluorescence studies, we examine excitation transport and trapping dynamics in photosystem I and the limitations imposed by the finite time resolution in single photon counting experiments. In particular, we show that rising components, associated with excitation transfer among different spectral forms, with lifetimes <20 ps would be undetected in a typical photon counting experiment.

INTRODUCTION

The initial steps in photosynthesis involve the transport and trapping of electronic excitations created by absorption of light. The trapping of the excitations by a reaction center leads to efficient charge separation and quenches the fluorescence of the donor molecules. Fluorescence decay measurements provide the means of determining the time scale(s) on which this process occurs. The ultimate goal of these experiments is to define the dynamics of this process in terms of the structural features of the light-harvesting system. Very little is known on a detailed level about the arrangement of individual pigment molecules in most antenna complexes, so the problem of relating experimental observations to specific structural features is difficult. A useful approach is to develop methods for simulation of excitation migration and to attempt to correlate the resulting fluorescence properties from model systems with structural features of the models. Comparison with experiments can then be made to evaluate a given model.

Calculations of excitation transport and trapping in photosynthetic systems using hopping models have appeared in several contexts. Studies of both regular lattices (1) and spatially random arrays (2) containing spectrally equivalent sites showed that in many cases the fluorescence decay curves consisted of a single exponential. This result was due, among other reasons, to a homogeneous initial condition (i.e., the excitation density on each site is equal at $t = 0$). In systems with a distribution of excited state energies, this condition is not realized experimentally. More recently Causgrove et al. (3) used a kinetic model based on the crystal structure of *Prostecochloris aestuarii* to describe excitation hopping between different subunits of the complex. In each of these studies the inhomogeneous nature of the absorption bands was not taken into account explicitly.

The absorption spectra of antenna systems are generally quite broad reflecting the presence of pigment molecules that absorb at a variety of different wavelengths. Even in complexes in which only one type of pigment exists, the spectra are statically broadened due both to pigment–pigment interactions and to different types of binding sites in the proteins that form the scaffolding for the pigment array. Once an excitation is created, it is not clear what effect, if any, spectral disorder plays in the migration of the excitations to the trap. Investigation of the effects of spectral disorder on the trapping dynamics in simple model systems is a major goal of this paper. It is important to establish the relation between this type of disorder and observable quantities such as fluorescence decay curves, time-resolved spectra, etc. In addition, we use our simulated decays to discuss the limitations of current methods of time-resolved fluorescence spectroscopy for the study of photosynthetic energy transfer.

A particular point of interest is the relation between the excitation spectra of individual decay components, obtained from fitting decay data to sums of exponentials, and the steady-state absorption spectrum of the array. It has been implicitly assumed in a number of studies of the

0006-3495/89/12/1203/13 $2.00

fluorescence decays of light harvesting arrays that the fluorescence excitation spectrum of a decay component is proportional to the absorption cross-section of that group of pigments that transfer energy to those pigments that are responsible for the decay component. This was quantified by Holzwarth (4) in the following relation for the amplitude of a component i.

$$A_i(\lambda_{exc}, \lambda_{em}) = C \cdot N \cdot \epsilon(\lambda_{exc}) \cdot k_{rad} \cdot F(\lambda_{em}). \quad (1)$$

Here $\epsilon(\lambda_{exc})$ is the absorption coefficient at the excitation wavelength, k_{rad} is the radiative rate, $F(\lambda_{em})$ is the normalized emission spectrum, and C is a constant. N is the number of pigment molecules that are connected to those molecules that contribute to that decay component.

We will show that in spectrally disordered systems, Eq. 1 holds only in the limit that the excitations are randomized among the different spectral types on a time scale fast compared to the fluorescence decay time. This is demonstrated by carrying out simulations of excitation hopping on two-dimensional lattices containing two or more site energies. The models we investigate are very crude models of real light harvesting arrays; however, the conclusions we draw from these studies have important implications in the interpretation of experimental data from real complexes. We emphasize this point by discussing our simulation results in light of recent time-resolved data from photosystem I (PSI) obtained in our laboratory (5–7).

MODEL SYSTEMS

We discuss several model systems chosen to illustrate the relation between the spatial arrangement of pigments and time-resolved excitation and emission spectra for systems containing more than one spectral form.

We start by considering the simple regular lattice (two-color) models shown in Fig. 1. Models 1–3 consist of two types of domains, each containing one spectral form of antenna pigment, but differing in the spatial organization of the domains. Each spectral form is assumed to have gaussian absorption and emission lineshapes. The domain containing the redder absorbing pigments also contains a centrally located trap at slightly lower energy which, when populated, can either detrap or lead to irreversible charge transfer. The wavelengths chosen correspond roughly to those found in core antenna complexes of PSI. The outer, or peripheral, regions contain pigments absorbing at bluer wavelengths. These models are thus "segregated" in the sense that different spectral types occupy different regions of the lattice. Each of the three models contain 80 pigments with absorption bands centered at 680 nm and 36 pigments with bands at 652 nm in addition to a trap at 700 nm. The spectral features are summarized in Table 1. A key feature of these models is that they each have the same absorption spectrum, which is shown in Fig. 2. The essential difference between them is the degree of connectivity between different spectral forms. In models 2 and 3, the number of 652-nm pigments with at least one 680 nearest neighbor is relatively small (nine and four, respectively). Exciting into the blue edge of the absorption band results in excitations that must make on the average an appreciable number of hops before they get redistributed among both spectral types. This should be contrasted to model 1, where the degree of connectivity between different forms is maximal.

These models have been constructed primarily to demonstrate important relations between steady-state and time-resolved spectra in a spectrally disordered system, rather than to mimic an actual photosynthetic light-harvesting complex. A slightly more realistic model, from a compositional point of view, is a regular lattice containing a larger variety of spectral forms, with a high degree of overlap of their absorption and emission spectra. Evidence of this comes from gaussian deconvolutions of antenna absorption bands (7, 8). Fig. 3 shows three multicolor models designed to aid in our interpretation of recent work on PSI antenna arrays in detergent-isolated

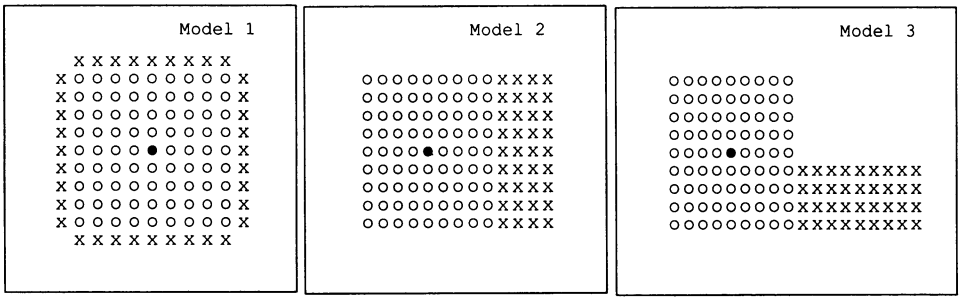

FIGURE 1 Model lattices containing two site energies. (X) Sites absorbing at 652 nm. (O) Sites absorbing at 680 nm. (●) Site absorbing at 700 nm (trap).

TABLE 1 Spectral properties of models 1–3

Spectral Type	Number	λ_{max} (abs.)	λ_{max} (em.)	FWHM
		nm	*nm*	cm^{-1}
x	36	652	667	700
o	80	680	695	700
o	1	700	715	700

complexes (6) and in PSII-minus mutants of *Chlamydomonas reinhardtii* (7). Like the two-color models, these three have identical absorption spectra, but differ in the degree to which the spectral disorder is spatially correlated. We give these models the names "funnel," random," and "trough" to reflect the manner in which sites of different spectral types are positioned with respect to one another. Table 2 shows the various spectral parameters used in our simulations of excitation transport on these lattices.

CALCULATIONS

Theory

We assume excitation transport to occur through an incoherent mechanism, i.e., a random walk. The equation of motion for the site occupation probabilities is the Pauli Master equation (9). If $p_i(t)$ is the probability that an excitation resides on the ith site at time t, then

$$dp_i(t)/dt = \sum_j F_{ij}p_j(t) - \sum_j F_{ji}p_i(t) - \tau_i^{-1}p_i(t), \quad (2)$$

where F_{ij} is the rate constant for transfer from pigment j to pigment i and $1/\tau_i$ is the rate for all decay processes other than energy transfer. In our calculations, τ_i is taken to be the fluorescence lifetime of free chlorophyll (~5 ns).

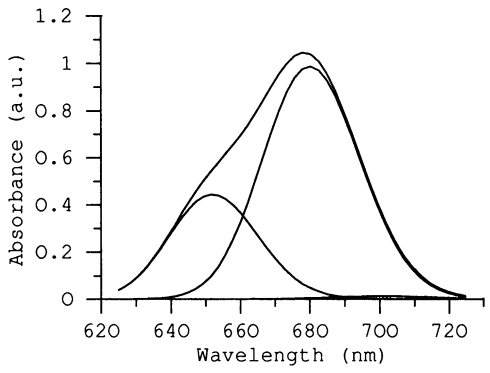

FIGURE 2 Absorption spectrum of each spectral type and total absorption of the array for models 1–3.

When i corresponds to the trap, τ_i is the time constant for charge separation. An excitation residing on the trap can suffer one of two fates: it can detrap or be irreversibly destroyed by charge transfer.

In our models not all sites are equivalent, which rules out an analytical solution. We therefore adopt the following simple numerical procedure. First, we write Eq. 2 in a more compact form.

$$\dot{\mathbf{P}}(t) = \mathbf{W} \cdot \mathbf{P}(t) \quad (3)$$

$\mathbf{P}(t)$ is the vector of site occupation probabilities and $\mathbf{W}$ is the $N \times N$ matrix of pairwise transfer rates. The matrix elements are given by

$$W_{ij} = (1 - \delta_{ij})F_{ij} - \delta_{ij}\sum_k F_{kj} - \delta_{ij}\tau_i^{-1}, \quad (4)$$

where δ_{ij} is the Kronecker delta. The structure of this matrix guarantees conservation of probability. This set of coupled first-order differential equations for the site occupation probabilities is easily solved, subject to the initial condition, $\mathbf{P}(0)$, to obtain

$$\mathbf{P}(t) = \exp(\mathbf{W}t) \cdot P(0) = \mathbf{G}(t) \cdot \mathbf{P}(0), \quad (5)$$

where $\mathbf{G}(t)$ is the Green's function for the system. Simulations of random models require that $\mathbf{G}(t)$ be averaged over a sufficient number of random configurations. For the random model discussed in Results and Discussion we have found that 15 configurations is sufficient to yield converged results. For the "segregated" models, we need only one configuration. For the relatively small number of sites considered here, it is convenient to express the Green's function in terms of the eigenvalues (λ_i) and eigenvectors ($\mathbf{M}_i$) of the rate matrix. This procedure guarantees that for a particular initial condition, the average over all possible random walks is computed exactly. The Green's function is given by

$$\mathbf{G}(t) = \mathbf{M}^{-1} \cdot \exp(\lambda t) \cdot \mathbf{M}, \quad (6)$$

where $\mathbf{M}$ is the matrix of eigenvectors and $\lambda = \mathbf{M} \cdot \mathbf{W} \cdot \mathbf{M}^{-1}$ is the diagonal matrix of eigenvalues. The matrix elements of $\mathbf{G}(t)$, $\mathbf{G}_{ij}(t)$, are interpreted as the conditional probability that an excitation starting at site j at $t = 0$ will be found on site i at time t. Thus $\mathbf{G}(t)$ evolves the initial distribution of excitations (created by optical absorption) into the distribution at time t. We are not particularly interested in the full vector $\mathbf{P}(t)$ because the individual site populations are not observable; rather what is observed is the fluorescence intensity as a function of time at various wavelengths. This depends on the probability that an excitation occupies a specific spectral type. We define the probability of finding the excitation on spectral type m regardless of position as

$$\mathcal{P}_m(t) = \Sigma' p_i(t), \quad (7)$$

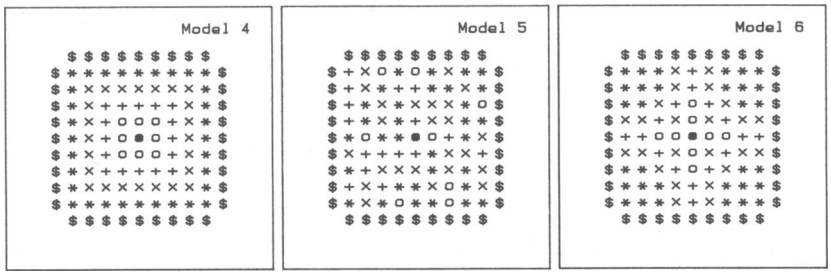

FIGURE 3 Model lattices containing six site energies. Symbols refer to spectral types listed in Table 3. Model 5 is a single example from the 15 configurations generated to calculate the average Green's function.

where the prime indicates summation over the set of pigments of spectral type m. The total fluorescence intensity is proportional to the probability that the excitation still resides on the lattice. If $I_m(\lambda_{em})$ is the emission lineshape of the mth spectral form, then the fluorescence decay at a particular wavelength is given by

$$I(\lambda_{em}, t) = \Sigma' P_m(t) \cdot I_m(\lambda_{em}). \quad (8)$$

The matrix elements of **W** are found by calculating the spectral overlap of the donor emission and acceptor absorption bands using the weak coupling theory of Förster (10). For convenience we assign gaussian absorption and emission lineshapes to the sites. The individual site spectra are defined by their width, σ, peak wavelength, λ, and transition dipole strength, μ. The Förster rate constant in units of picoseconds^{-1} for two sites whose donor emission and acceptor absorbance maxima are separated by Δ centimeters^{-1} is

$$F_{ij} = \frac{4\pi(10^{-24})\kappa^2}{ch^2n^4R_{ij}^6} \frac{\mu_i^2\mu_j^2}{\sqrt{2\pi\sigma_i\sigma_j}} \left(\frac{1}{2\sigma_i^2} + \frac{1}{2\sigma_j^2}\right) \exp \cdot \left[\frac{-\Delta_{ij}^2}{4\sigma_i^2\sigma_j^2}\left(\frac{1}{2\sigma_i^2} + \frac{1}{2\sigma_j^2}\right)^{-1}\right], \quad (9)$$

where n is the refractive index, κ^2 the orientation factor, and R_{ij} the distance between the sites.

For any pair of spectrally inequivalent sites, we calculate the rate constant for the faster (i.e., the "downhill") rate using Eq. 9. The reverse rate is calculated from the downhill rate using the detailed balance condition, $F_{ij} = F_{ji} \exp(-\beta\delta A ij)$, where $\delta A ij$ is the difference between the peak frequencies of the two absorption (or emission) bands. This assures that in the absence of trapping, the site populations relax to a Boltzmann distribution.

TABLE 2 Spectral properties of models 4–6

Spectral Type	Number	λ_{max} (abs.)	λ_{max} (em.)	FWHM
		nm	*nm*	cm^{-1}
o	1	700	707	700
o	8	695	702	700
+	16	690	697	700
x	24	685	692	700
*	32	680	687	700
$	36	672	679	700

Simulations

Our strategy for simulating the transport dynamics of our models is simple. We first produce an initial condition by specifying the excitation wavelength. This is done by calculating the contribution of each spectral type to the total absorption cross-section and distributing the probability density equally among sites of the same spectral type in a manner commensurate with that spectral type's cross-section at the excitation wavelength. We generate the rate matrix by using Eqs. 4 and 9, the spectral parameters in Tables 1 and 2, and by assuming nearest neighbor coupling. This restriction can be easily lifted and does not change the qualitative conclusions of our work. Numerical diagonalization of **W** allows the fluorescence intensity at different pairs of excitation and emission wavelengths to be calculated. We can think of these intensities as being points on an excitation-emission surface, $I(\lambda_{exc}, \lambda_{em}, t)$. Cross-sections of these surfaces obtained by holding any two parameters constant yield important information concerning the dynamics of transport. A series of such surfaces was calculated at 5-ps time intervals. We fit the various decays to sums of exponentials using global data analysis (11). This procedure is based on the assumption that the "correct" decay law should contain time constants that are independent of the excitation and emission wavelengths.

An open question is whether the parameters obtained from fitting data to sums of exponentials can be related to any physical aspect of the dynamics. The true decay law, of course, is given by Eq. 6, which contains N time constants (i.e., reciprocals of the eigenvalues of **W**). In reality only a few of these eigenvalues contribute to the

long-time behavior, which is observed experimentally, suggesting that fitting to an expression containing two or three exponentials is not necessarily unrealistic. Other methods of data analysis in these types of problems have been recently discussed (12). In the global procedure, we choose to constrain the time constants to be invariant across the emission direction for a given excitation wavelength. Thus for each emission surface we obtain a set of time constants that represent the optimum decay law. In principle, these time constants should also be invariant along the excitation direction, however, practical considerations pertaining to the analysis routine mandate that we carry out independent fits at each excitation wavelength. Examination of the time constants obtained by this procedure reveals that, except for the case of very short components (<10 ps), the lifetimes show virtually no variation across the excitation direction, indicating our decay law is valid over the wavelength ranges we have studied. Thus for a given model the emission intensity has the form

$$I(\lambda_{exc}, \lambda_{em}, t) = \sum_i A_i(\lambda_{exc}, \lambda_{em}) \exp(-t/\tau_i). \quad (10)$$

The amplitudes corresponding to the time constants have dependence on both excitation and emission wavelengths. From them we can generate excitation and emission spectra for each component by normalizing the decays to the relative absorption intensity at the excitation wavelengths. Steady-state spectra are obtained by integrating over time.

$$I(\lambda_{exc}, \lambda_{em}) = \int I(\lambda_{exc}, \lambda_{em}, t)\, dt = \sum_i A_i(\lambda_{exc}, \lambda_{em})\tau_i. \quad (11)$$

For all simulations, we have chosen transition dipole strengths, spectral linewidths, etc., to be similar to those of chlorophyll *a*. The orientation factor is set to 2/3, the static average, which allows us to focus strictly on the effects of spectral disorder. The presence of orientational disorder may also be an important factor in determining trapping times in real systems. Both types of disorder may lead to preferred pathways (and bottlenecks) to the trap region. The lattice spacing, 12 Å, is chosen to be such that the time constant for transfer to a neighboring site is ~1 ps. The average amount of time an excitation stays on a site once it reaches it is the inverse of the product of the coordination number of the lattice and the rate, in this case ~250 fs. This is similar to that obtained from analysis of PSI data (5) using the model of Pearlstein (1). The electron transfer rate used was 0.37 ps^{-1}, which is approximately the value observed experimentally in both bacterial reaction centers (13) and isolated reaction centers of PSII (14). This is also similar to the value obtained from a regular lattice model analysis of PSI data (5).

RESULTS AND DISCUSSION

Two-color models

We begin our discussion by considering models 1–3. As mentioned earlier, each array has the same absorption spectrum, but different spatial features. We want to explore the relationship between the excitation spectra of individual decay components and the steady-state spectrum.

In our model systems, all pigments are connected so N in Eq. 1 is just the total number of pigments in the array, namely 117. An immediate prediction from Eq. 1 is that excitation spectra depend only on the number of pigments and not on the specifics of energy transport. The geometrical differences introduced in the segregated models are designed to test this ansatz. An excitation starting out in the 652-nm region must execute on the average a progressively longer random walk until it reaches the 680-nm region as one goes from model 1 to model 3. One might suppose that an important consideration is the amount of time it takes for the excitation to visit a representative sample of spectral types. This randomization process eventually leads to equilibration of the excitations on the lattice provided the trapping time is substantially slower than the single-step transfer time. Experimentally the time scale of the equilibration can be determined by monitoring the time-dependent evolution of the total emission from all components. Once randomization is complete, the spectral lineshape will resemble that of the steady-state spectrum.

To test this idea we have carried out simulations on these models using various excitation wavelengths. The emission surfaces obtained were fit to a sum of two exponentials, except for model 3, which required three exponentials. In all our fits, we constrained the lifetimes to be constant across the surface. Also, on models 2 and 3, we fit each decay curve separately to the same number of exponentials to examine the wavelength dependence of the lifetimes. We found that the lifetimes varied by <5% across the surfaces, indicating our decay laws were accurate for the region of interest.

The time constants obtained from our simulations are shown in Table 3. To determine which components corresponded to trapping of the excitation, we carried out similar calculations using a value for the charge transfer rate that was an order of magnitude less than used previously. For each model, the largest time constant was the only one sensitive to this rate. The others correspond to motion of the excitation between different spectral forms. The trap-sensitive time constant was found to be 62 ps for models 1 and 2 and 64 ps for model 3. For model 1, a short time component of ~1 ps was seen, which is approximately the single step transfer time. This is not

TABLE 3 Time constants obtained from fitting results from models 1–3

Model	τ_1	τ_2	τ_3
	ps	*ps*	*ps*
1	1.2 ± 0.1	62.0 ± 0.02	—
2	8.1 ± 0.3	62.2 ± 0.05	—
3	2.4 ± 0.3	63.9 ± 0.05	39.7 ± 0.2

The decay expression is $I(\lambda_{exc}, \lambda_{em}) = \Sigma A_i (\lambda_{exc}, \lambda_{em}) \exp(-t/\tau_i)$. Error bars represent standard deviations from the results of global fits at 15 excitation wavelengths.

surprising from a model with such a high degree of connectivity between the two types of sites. Model 3 exhibits an intermediate component with a lifetime of 40 ps which does not depend on the internal dynamics of the trap. The short components in each model arise from the set of pigments that has a nearest neighbor of a different color. The 40-ps component thus comes from the relatively large number of pigments in the 652 domain which are remote from the spectral boundary. We surmise that the 8-ps component of model 2 probably results from an average of a longer lifetime component and an unresolved component reflecting the single step transfer time. It is interesting to note the similarity between this value and that obtained by Knox and Lin (15) for the fast decay component (9 ps) in low-temperature fluorescence measurements of PSII.

We now move to analysis of the amplitudes corresponding to these time constants and focus on excitation spectra. The amplitude of each component as a function of excitation wavelength is shown at various emission wavelengths in Fig. 4. There is a marked difference between excitation spectra at the same emission wavelength for the different models. Negative amplitudes represent risetimes in the fluorescence decays when excited at the particular λ_{exc}. In each case the amplitude of the trap-sensitive component is everywhere positive, as it should be. In model 1, where excitations, regardless of where they originate, are rapidly randomized among the two spectral forms, the excitation spectrum of the component 2 (62 ps) tracks the absorption spectrum very closely (Fig. 4, *b* and *d*), while the excitation spectrum of the component 1 (Fig. 4, *a* and *c*) resembles the negative of the absorption lineshape of the 652-nm pigments. For model 2 we see qualitatively similar spectra, however, the excitation spectra overestimate intensity in the bluer end of the band due to the fact that excitations spend a substantially longer time in the 652-nm region. This is further exemplified in model 3 where the increased length of the random walks in the 652-nm domain leads to an excitation spectrum of the slow component that bears no resemblance to the absorption spectrum of the array. The presence of slow spectral randomization leads to a break-

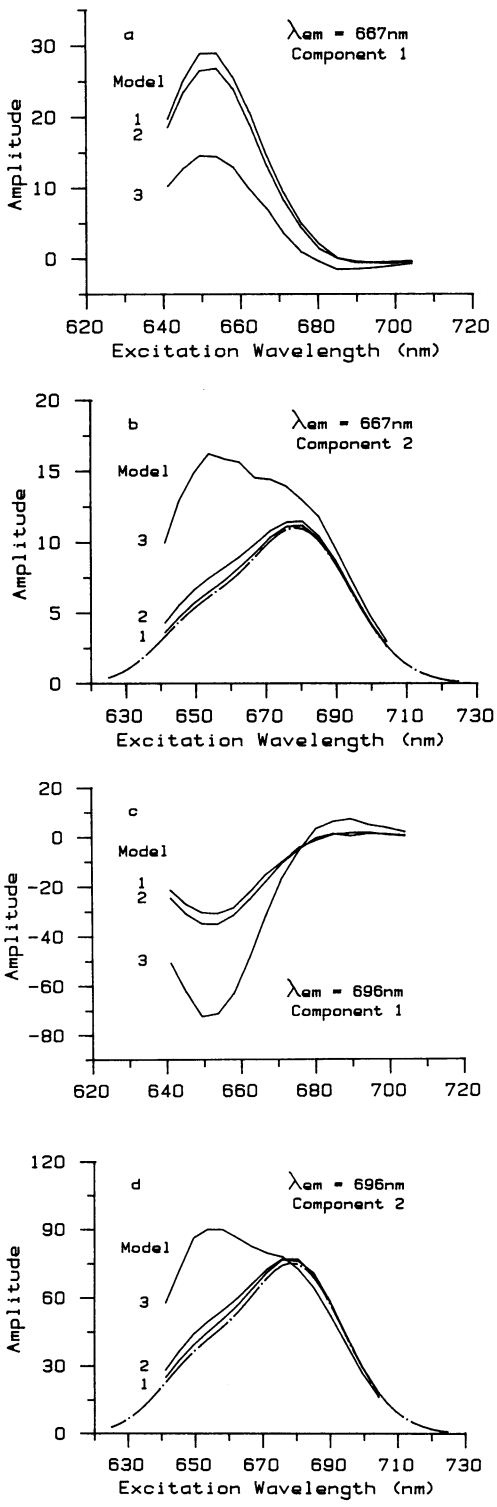

FIGURE 4 Fluorescence excitation spectra of individual components of the decay for models 1–3. The time constants are shown in Table 2. (*a*) Component 1, λ_{em} = 667 nm. (*b*) Component 2 (trap-sensitive), λ_{em} = 667 nm. (*c*) Component 1, λ_{em} = 696 nm. (*d*) Component 2, λ_{em} = 696 nm.

down of the simple relation (Eq. 1) between the number of pigments in the array and the excitation spectra of the various decay components. In the limit of fast randomization, this relation holds. We demonstrate this by taking model 1 and reducing by half the number of 652-nm pigments present (in this case by deleting two opposing rows), and calculating the excitation spectra for the resulting amplitudes. As is expected, the excitation spectrum again mirrors the absorption spectrum of the array (not shown).

The difference in spatial arrangements of the pigments is also reflected in the calculated fluorescence excitation spectra, summed over all components. A comparison of these for models 1–3 is shown in Fig. 5. For model 3, the lifetime of the 40-ps component contributes significantly to the steady-state spectra, giving an excitation spectrum that depends quite strongly on the emission wavelength. This emission wavelength dependence of the spectral lineshape decreases progressively as the rate of randomization among the antenna spectral forms increases (model 3 → model 1). In the limit of fast randomization, the normalized excitation spectra are identical at each emission wavelength (not shown). Similar behavior is seen on the emission side. Fig. 6 shows steady-state emission spectra at various excitation wavelengths for the three models. Clearly, slow spectral randomization yields emission spectra that are much more sensitive to excitation wavelength than those corresponding to systems in the fast randomization limit.

In our previous studies of fluorescence decay in PSI (6, 7), we observed that all samples containing coupled peripheral antenna complexes (detergent-isolated complexes and *C. reinhardtii* mutants) exhibited an intermediate decay component (τ = 200–400 ps) that accounted for 10–30% of the total decay. The excitation spectrum of this component had characteristics of both peripheral and core antenna pigments, whereas the emission spectrum was that of the core antenna pigments only. Because there was no risetime associated with this decay, we could not attribute it to energy transfer between antenna spectral forms. By analogy to the 40-ps decay component seen in model 3, it is possible that the intermediate decay in PSI arises as a result of slow spectral randomization between the peripheral and core antennas. Our inability to detect risetimes associated with peripheral to core antenna transfer using single photon counting will be addressed in the following section.

Multicolored models

In the previous section, we used simple two-color models with low spectral overlap between pigment absorptions to demonstrate two important points: (*a*) the wavelength dependence of the amplitudes derived from global fits

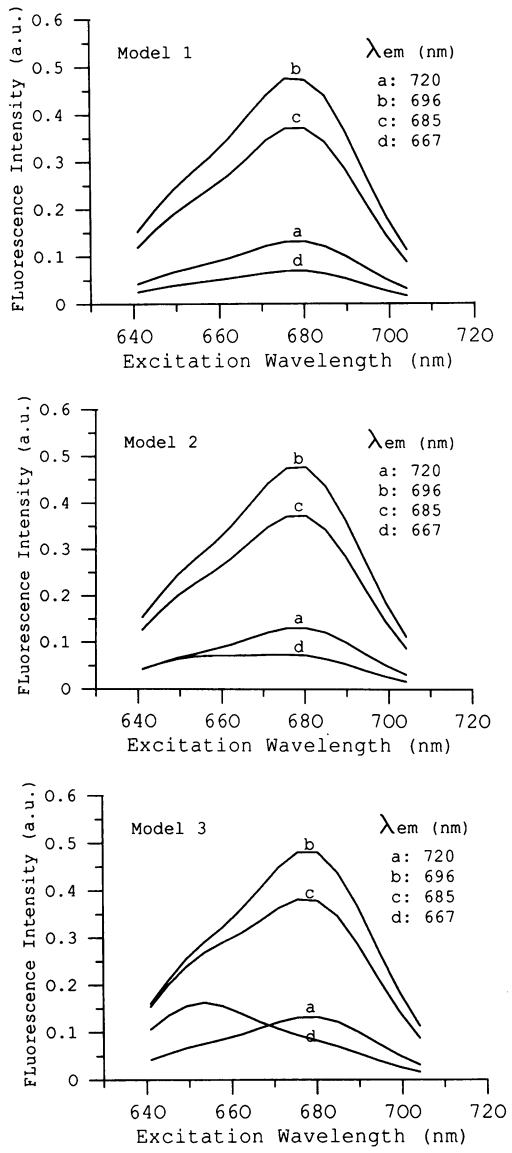

FIGURE 5 Steady-state fluorescence excitation spectra for models 1–3 at emission wavelengths: λ_{em} = 720, 696, 685, and 667 nm.

cannot be divorced from the dynamics of the excited state in the pigment array; and (*b*) the dynamics should be determined by both spectral and spatial characteristics of the array. We now consider three additional models (Fig. 3) that use the same lattice configuration as model 1 but contain five antenna spectral forms. The spectral properties of these models (Table 3) were chosen to mimic the chlorophyll *a* pigments in the peripheral (LHC I) and core antenna complexes of photosystem I. Again the models have identical absorption spectra by virtue of the number of sites occupied by each spectral type. The absorption spectrum of each spectral and the total absorption spectrum of the array is shown in Fig. 7. We will

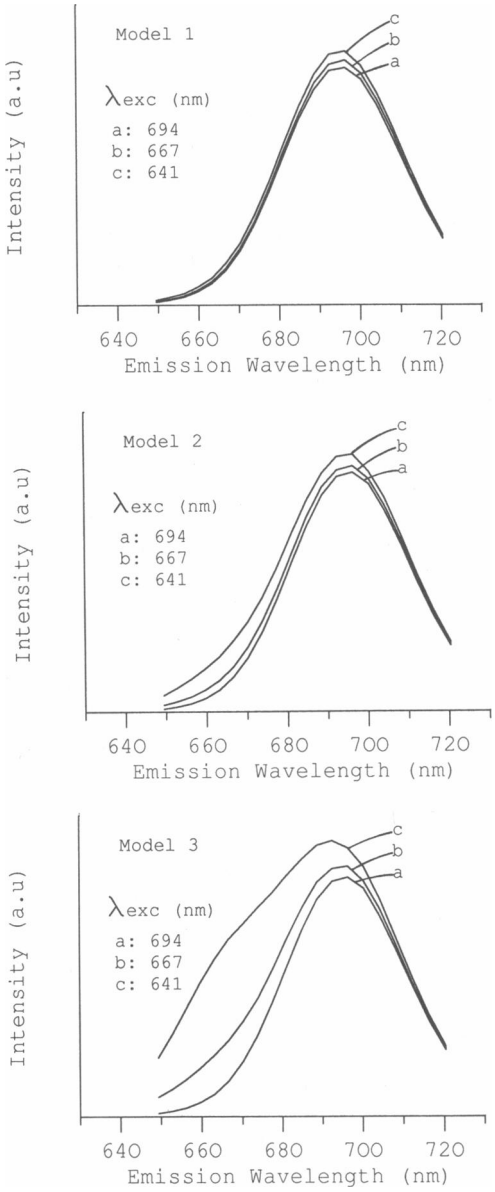

FIGURE 6 Steady-state emission spectra for models 1–3 at excitation wavelengths: λ_{exc} = 694, 667, and 641 nm.

build on the ideas developed in the previous section making reference to our recent results (5–7) from fluorescence studies of trapping dynamics in isolated PS I complexes and in mutants of *Chlamydomonas reinhardtii* lacking PS II. In particular, we will address three points: (*a*) the effects of increased spectral overlap between antenna forms on the excited state dynamics, (*b*) the ability of the model simulations to aid in interpretation of data from our previous studies, and (*c*) the limitations imposed by the finite time resolution of fluorescence detection techniques.

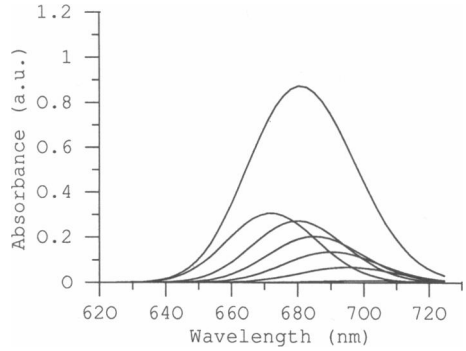

FIGURE 7 Absorption spectra of each spectral form and total absorption of the array for models 4–6.

Before considering the results of these models, we briefly review the relevant data and conclusions from our experimental studies on PS I. For detergent-isolated PS I reaction center/core antenna complexes, the lifetime of the dominant, short component (10–40 ps) was found to vary linearly with the core antenna size in accord with the simple lattice model of Pearlstein (1). The lifetime of this component is limited by efficient photochemical quenching on P700. A second, 5–6–ns component was assigned to core antenna aggregates lacking a functional trap. The relationship between lifetime of the trapping-dependent component and the core antenna size was extended to include in vivo measurements on wild-type and PS II-minus mutants of *C. reinhardtii*. In addition we noted that the steady-state spectral properties of isolated PS I complexes did not vary with antenna size, were similar to the time-resolved emission spectrum of the trapping-dependent component and that the lifetime of the trapping-dependent component was constant for all excitation wavelengths in the core antenna absorption. Taken together, these data suggested that the excited state is equilibrated among the core antenna spectral forms during its lifetime. This was confirmed by direct analysis of the emission at reciprocal excitation/emission wavelength pairs (7). We therefore concluded that these data argue against a "funnel" organization of the core antenna.

In all our previous measurements, fluorescence decays were fit to a sum of exponentials at individual excitation/emission wavelength pairs (no global analyses). With this type of analysis, we consistently observed a dependence of the trapping-dependent lifetime on excitation and emission wavelength. In the detergent-isolated complexes lacking chl *b*, the lifetime of the short decay component was constant at emission wavelengths shorter than the trap absorption at 700 nm but increased at longer wavelengths. This behavior was independent of excitation wavelength. In *C. reinhardtii*, the emission wavelength dependence was found to be quite different, with the

lifetime increasing at wavelengths up to 700 nm and constant at longer wavelengths. The lifetime of the trapping-dependent component was also independent of excitation wavelength at wavelengths dominated by core antenna absorption but increased by 5–20 ps in the region of LHC I absorption. As a corollary to these observations, we were unable to detect risetimes associated with excitation transfer between LHC I and the core antenna or among spectral forms in the core complex.

In models 4–6, we have chosen the outermost pigments to represent chl *a* of the peripheral (LHC I) antenna (absorption maximum, 672 nm). The remaining antenna pigments have absorptions and relative numbers that approximate the PS I core antenna. To kinetically distinguish excited state transfer between peripheral and core pigments from transfers within the core, we have set the transfer time between the 672-nm pigments and their nearest neighbors to be 8 ps by altering the oscillator strength of the 672 pigments. This transfer time is similar to that postulated in reference 7. The distinctions between models 4, 5, and 6 are in the symmetry of the arrangement of the core antenna spectral types. The funnel model (No. 4) is arranged so that as one moves radially out from the trap, the absorption spectrum of the individual pigments becomes progressively bluer. The trough model (No. 6) also exhibits a spatial correlation of the spectral broadening; however, it is of quite a different nature. Here the redder pigments are arranged so as to form troughs, or corridors, which serve to rapidly transfer excitations into the trap region. For the random model (No. 5), the decays were averaged over 15 configurations.

We have calculated the emission surfaces for models 4–6 using a time step of 5 ps. The time constants obtained from the data (Table 4) show that in each case the decays are described by two exponential components. Attempts to model the data with three or more exponentials did not statistically improve the fits. For all three models, the shorter (7 ps) lifetime corresponds to the transfer time between peripheral and core pigments while the longer lifetime is sensitive to the photochemical rate. For the two models in which there is a symmetrical arrangement of core pigments, the lifetime of the trapping-sensitive component is nearly identical (78 ps). In the random model, the trapping-sensitive lifetime increased to >100 ps. In the symmetric core models (4 and 6), we expect that the first passage time is shorter because the spectral arrangement biases the random walk toward the trap. It has been argued that this would lead to more efficient trapping (16); however, in such arrangements the probability of detrapping will also increase and the resulting dynamics may be very sensitive to the photochemical rate (17). The 35% increase in the trapping time that we observe in going from an ordered to a random arrangement of spectral forms indicates the importance in this case of fewer favorable transfer pathways to the trap compared to the decreased detrapping rate.

In models 1–3, the substantial energy gap between the two spectral forms led to fluorescence risetimes with appreciable amplitudes. The existence of these risetimes produced excitation spectra for the individual components that did not track the absorption spectra. In models 4–6, the degree of overlap between spectral forms is much greater. Our inability to detect these risetimes (using convoluted data; see below) in the global fits suggests that the greater spectral overlap has reduced the amplitudes of risetimes associated with transfer among differing spectral forms.

Calculated excitation spectra for the trapping-dependent decay component in all three models closely follows the steady-state absorption spectrum (Fig. 8 *a*). By analogy to models 1–3, this suggests that the excited state reaches a rapid equilibrium among the core spectral forms. The similarity of the dynamics in models 4–6 may be demonstrated by examining the time-resolved emission spectrum from all pigments at various times after excitation at wavelengths absorbed primarily by the peripheral

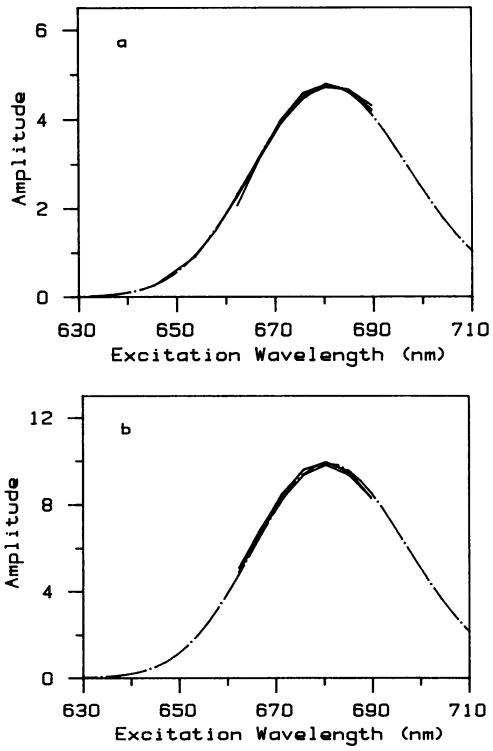

FIGURE 8 Fluorescence excitation spectra of component 2 (trap-sensitive) for models 4–6. λ_{em} = 720 nm. (*a*) Data without convolution. (*b*) Data convoluted with 60 ps instrument response function. The absorption spectrum of the array (—·—·—) is shown for comparison.

antenna. Fig. 9 shows the normalized emission spectrum at 0, 5, 10, 15, 20, and 30 ps using 662 nm excitation. The time evolution of the emission spectra is virtually identical in all three models and the data indicate that, in each case, the excitation is equilibrated among all core antenna spectral forms in <20 ps. Because the time resolution of the global fits is limited by the 5-ps steps used in calculating the emission surfaces, the similarities between these results suggests that experiments with time resolution limited to tens of picoseconds cannot determine the relationship between spectral form and spatial position in antenna systems with substantial overlap between site

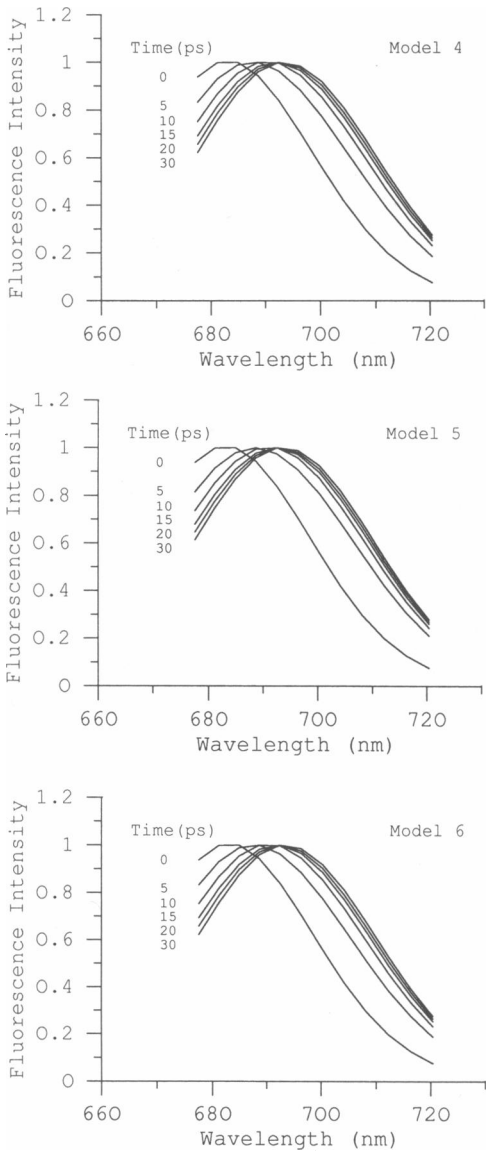

FIGURE 9 Time-resolved emission spectra at 0, 5, 10, 15, 20, and 30 ps for models 4–6. Spectra have been normalized to correct for trapping. Excitation wavelength, 662 nm.

energies. This also suggests that fluorescence upconversion experiments with subpicosecond resolution may be a useful probe of the antenna structure and excitation dynamics.

The results from models 2 and 4–6 demonstrate that finite time resolution can limit our ability to extract information from the calculated fluorescence emission surfaces. In laboratory experiments, further limitations may be imposed by the necessity to convolute data with an instrument response function. To demonstrate the effects of both of these limitations, we have carried out a study of simulated decay curves composed of three exponentials, one of which has a negative amplitude. We chose lifetimes of 8, 80, and 2,000 ps (amplitudes of −0.50, 1.40, and 0.10, respectively) to approximate in vivo decays associated with coupled LHC I, PS I core, and uncoupled LHC I complexes. After addition of gaussian noise, the simulated decay was convoluted with a real photon counting instrument response function of ~60 ps FWHM. The resulting fit (662 nm excitation, 696 nm emission, Fig. 10 *a*) shows that although the two longer lifetime components were accurately fit, the 8 ps rising component went undetected. The excellent reduced chi-squared value (0.98) and the distribution of residuals provide no suggestion of an additional component. We conclude, based on the reduced chi-squared values for fits with and without the short component, that a risetime of <20 ps would be undetected in a typical photon counting measurement.

For comparison we repeated the same simulated decay calculated at 0.2-ps intervals and convoluted with an autocorrelation function of 0.8 ps FWHM (from our subpicosecond amplified dye laser system). Attempts to fit this data to a single exponential yielded a suboptimal chi-squared value (1.34) and a nonrandom distribution of residuals (Fig. 10 *b*). In addition, the resulting lifetime (117 ps) appears to be increased due to the unresolved contribution of the rising component. These data are in agreement with our previous supposition that the 5–20 ps increase in PS I core lifetime at laser wavelengths that primarily excite peripheral LHC I pigments was the result of an unresolved lifetime (<5 ps) associated with excitation transfer from peripheral to core pigments (7). When the higher resolution simulation data is fit to a two exponential decay (Fig. 10 *c*), the nonlinear least squares routine returns the correct lifetimes and amplitudes, again suggesting that fluorescence upconversion experiments should provide a more detailed picture of excitation dynamics in real systems.

The emission surfaces calculated from models 4–6 (5-ps steps, no convolution with an instrument response function) were all fit quite well by global analysis to two exponentials, with the longer lifetime corresponding to the trapping-sensitive component. A risetime of 8 ps was also detected in each case (Table 4). Fitting the data to

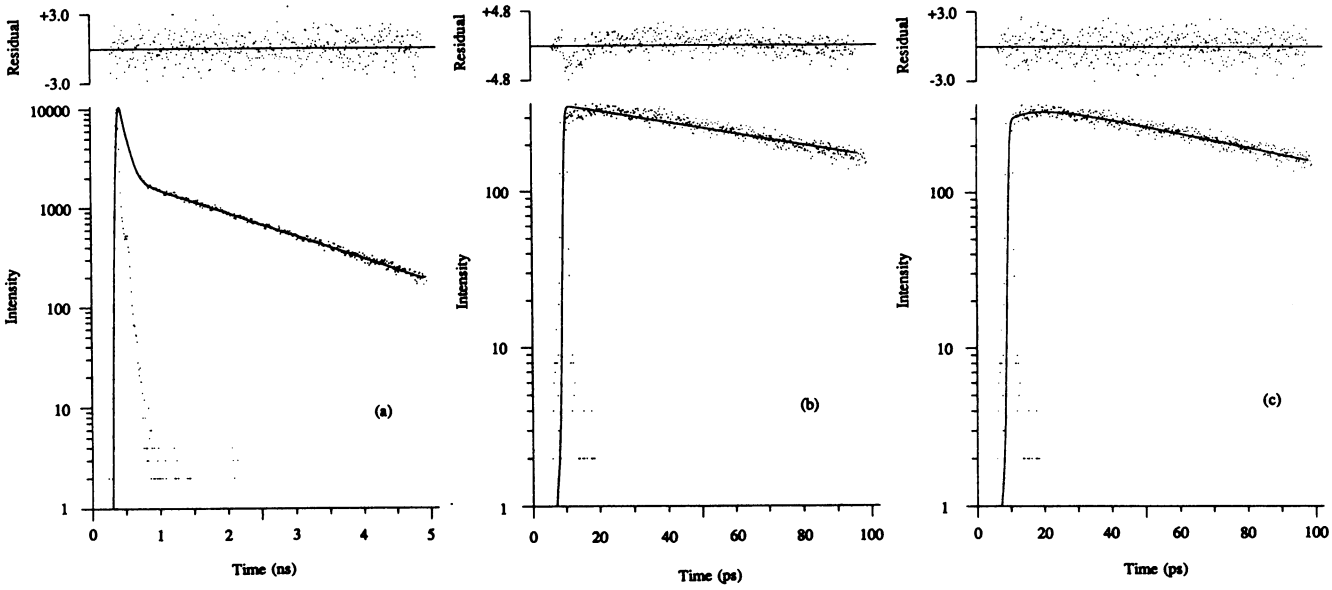

FIGURE 10 Fluorescence decay curve from model 6 (trough). The lifetimes are shown in Table 4. Excitation and emission wavelengths are 662 and 696 nm, respectively. A 2-ns component (relative amplitude, 10%) has been added to represent disconnected chlorophylls. (*a*) Data convoluted with 60 ps instrument response function; fit to double exponential. $A_1 = 89.0\%$, $\tau_1 = 79.5$ ps, $A_2 = 11.0\%$, $\tau_2 = 1997.3$ ps; $\chi^2 = 0.98$. (*b*) Data convoluted with 800 fs (FWHM) instrument response function; fit to single exponential. $A = 100\%$, $\tau = 117.4$ ps; $\chi^2 = 1.34$. (*c*) Data convoluted with 800 fs instrument response function; fit to double exponential. $A_1 = -46.5\%$, $\tau_1 = 7.9$ ps, $A_2 = 146.5\%$, $\tau_2 = 93.0$ ps; $\chi^2 = 0.99$. In *b* and *c*, the time step in the simulation was 200 fs, and the 2-ns component was not included in the fit due to the limited time range of the data. A negative amplitude represents a risetime.

three exponentials did not reduce the chi-squared values or change the distribution of residuals. However, in this case there is no lengthening of the lifetime because of the unresolved risetime. The fluorescence excitation spectra calculated from the convoluted fits (Fig. 8 *b*) are nearly identical for the three models and are in good agreement with the absorption spectrum. This suggests that the high degree of overlap between spectral types ensures significant equilibration of the excitation among spectral forms even when transfer between two forms is slowed by other factors (in this case, reduced oscillator strength). However, in analysis of PS I decays in *C. reinhardtii* mutants lacking PS II (7), we were unable to produce excitation spectra that were even qualitatively similar to the absorption spectra. In all cases, the bandwidth of the excitation spectrum for the dominant, trapping-sensitive component was about one-half that of the absorption spectrum (Owens, T. G., unpublished data).

TABLE 4 Time constants obtained from fitting results from models 4–6 to the expression $I(\lambda_{exc}, \lambda_{em}) = \Sigma A_i \cdot (\lambda_{exc}, \lambda_{em}) \exp(-t/\tau_i)$

Model	τ_1	τ_2	Convoluted τ	Convoluted χ^2
	ps	*ps*	*ps*	*ps*
4	7.1 ± 0.4	77.6 ± 0.04	78.7 ± 0.4	1.06 ± 0.01
5	6.6 ± 0.3	105.7 ± 0.7	107.0 ± 0.8	1.05 ± 0.02
6	7.1 ± 0.4	78.8 ± 0.03	79.9 ± 0.4	1.02 ± 0.03

Error bars represent standard deviations from results of global fits at seven excitation wavelengths. The values in the two righthand columns were obtained by convoluting our data with an instrument response function of 60 ps and fitting to a single exponential using a routine with a variable shift parameter.

Experimentally it is known that the lifetime of the trapping-sensitive component in PS I varies with both excitation and emission wavelength (6, 7). This variation has been attributed to several factors including the presence of spectrally resolved but temporally unresolved decays with similar lifetimes (18) and increasing lifetimes of excitations with energies lower than that of the trap (6). Our simulations also suggest that such behavior may result from fitting data to decay laws containing too few components. We expected that in our fits to models 4–6 using the decays convoluted with photon counting instrument response functions, that the lifetime of the trapping-sensitive component would depend on both excitation and emission wavelength. The data (Fig. 11) show that in all cases the lifetime obtained by exciting in the higher energy pigments is seen to increase with emission wavelength up to 700 nm and then to level off. The excitation wavelength dependence shows the opposite behavior

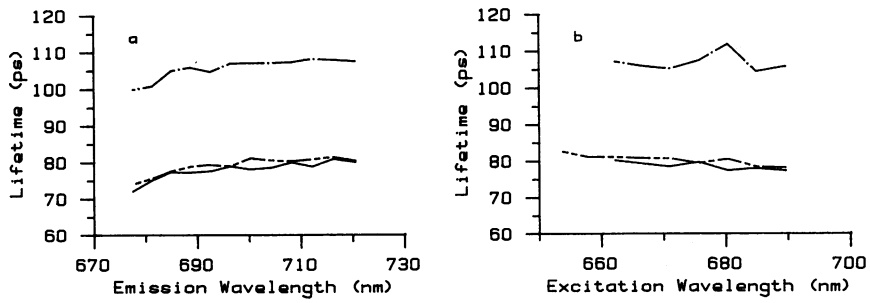

FIGURE 11 Lifetime of the trap-sensitive component for models 4–6 as a function of (*a*) emission wavelength and (*b*) excitation wavelength. (—) funnel; (—·—·) random; (– – –) trough.

though the changes are smaller. These trends are qualitatively similar to those measured in fluorescence studies of *C. reinhardtii* mutants lacking PS II (7). Thus, limited temporal resolution in photon counting experiments may also result in lifetime variations with wavelength. Throughout these simulations, we have observed good agreement between the lifetimes and amplitudes obtained from global analysis (assuming that lifetimes are independent of emission wavelength) and analogous parameters determined at discrete excitation and emission wavelength pairs. However, the inherent limitations in experimental data introduced by finite temporal resolution and the necessity of deconvoluting instrument response functions suggest that the results of both discrete and global analysis must be interpreted with care. Continued application of simulation techniques should further quantify these limitations and aid in the interpretation of experimental data.

CONCLUSION

We have shown that in general there is no simple relation between fluorescence excitation spectra and steady-state absorption spectra in spectrally disordered systems. The wavelength dependence of the amplitudes cannot be divorced from the dynamics of excitation transfer. Only when excitations are rapidly randomized among all spectral types does the excitation spectrum for a particular decay component accurately reproduce the absorption spectrum of all pigments efficiently coupled to the emitting species. We stress that the important factor is not the time scale of spectral equilibration, rather it is the time scale on which the excitations visit a representative sample of the various spectral forms. In the former, excitations must spend an amount of time on a given spectral form that is commensurate with that form's Boltzmann factor, whereas in the latter no such condition is imposed. Indeed, it is quite possible that in many systems thermal equilibrium among the N excited states is never realized due to the finite lifetime of the excitations.

Moreover, it was established that the finite time resolution and the necessity of convoluting decay curves with an instrument response function can both obscure short lifetime components corresponding to energy transfer between spectral forms of the antenna and lead to erroneous estimates of the number of pigments contained in the antenna pool.

Our simulations of energy transfer in the core antenna of crude models of PSI demonstrate that rapid randomization or equilibration of an excitation among a representative distribution of core antenna spectral forms is a consequence of the strong spectral overlap of the different spectral forms and need not be related to the spatial properties of the array. However, distinction between the limiting cases of antenna organization (random vs. funnel models) may be experimentally accessible using subpicosecond techniques such as fluorescence upconversion. The simulations also indicate that our inability to observe fast risetimes associated with energy transfer between peripheral and core spectral forms is a consequence of limited time resolution and deconvolution of instrument response functions. Similarly, the excitation and emission wavelength dependence of decay lifetimes seen in previous studies is, at least in part, a consequence of these limitations. Finally, restrictions in the number of paths of excitation transfer between coupled antenna pools result in slow spectral randomization, biexponential transfer kinetics between the pools, and significant deviations between the time-resolved excitation and steady-state spectra.

We thank J. M. Beechem for supplying the global analysis fitting routine.

This work was supported by grants from the National Science Foundation to G. R. Fleming (DMB 8509590) and to T. G. Owens (DMB 8803626).

Received for publication 15 May 1989 and in final form 28 July 1989.

REFERENCES

1. Pearlstein, R. M. 1982. Exciton migration and trapping in photosynthesis. *Photochem. Photobiol.* 35:835–844.
2. Shipman, L. L. 1980. Excitation migration in photosynthetic systems on the picosecond timescale. *Photochem. Photobiol.* 31:157–167.
3. Causgrove, T. P., S. Yang, and W. S. Struve. 1988. Polarized pump-probe spectroscopy of exciton transport in bacteriochlorophyll a-protein from prosthecochloris aestuarii. *J. Phys. Chem.* 92:6790–6795.
4. Holzwarth, A. R. 1987. A model for functional antenna organization and energy distribution in the photosynthetic apparatus of green plants and green algae. *In* Progress in Photosynthesis Research. Vol. 1. J. Biggins, editor. Martinus Nijhoff, The Hague. 53–60.
5. Owens, T. G., S. P. Webb, L. Mets, R. S. Alberte, and G. R. Fleming. 1987. Antenna size dependence of the fluorescence decay in the core antenna of photosystem I: estimates of charge separation and energy transfer rates. *Proc. Natl. Acad. Sci. USA.* 84:1532–1536.
6. Owens, T. G., S. P. Webb, R. S. Alberte, L. Mets, and G. R. Fleming. 1988. Antenna structure and excitation dynamics in photosystem I. I. Studies of detergent isolated photosystem I preparations using time-resolved fluorescence analysis. *Biophys. J.* 53:733–745.
7. Owens, T. G., S. P. Webb, L. Mets, R. S. Alberte, and G. R. Fleming. 1989. Antenna structure and excitation dynamics in photosystem I. II. Studies with mutants of *Chlamydomonas rheinhardtii* lacking photosystem II. *Biophys. J.* 56:95–106.
8. Shiozawa, J. A., R. S. Alberte, and J. P. Thornber. 1974. The P700-chl a-protein. Isolation and some characteristics of the complex in higher plants. *Arch. Biochem. Biophys.* 165:388–397.
9. Schuler, K. E., G. H. Weiss, and I. Oppenheim. 1977. Stochastic Processes in Chemical Physics. MIT Press, Cambridge, MA.
10. Förster, Th. 1965. Delocalized excitation and excitation transfer. *In* Modern Quantum Chemistry. Vol. III. O. Sinanoglu, editor. Academic Press, Inc., New York. 93–137.
11. Knutson, J. R., J. M. Beechem, and L. Brand. 1983. Simultaneous analysis of multiple decay curves: a global approach. *Chem. Phys. Lett.* 102:501–507.
12. Byers, J. D., M. S. Friedrichs, R. A. Friesner, and S. E. Webber. 1989. Polymer structure and down-chain electronic energy transfer. *In* Molecular Dynamics in Restricted Geometries. J. Klafter and J. Drake, editors. John Wiley & Sons, New York. 99–144.
13. Fleming, G. R., J.-L. Martin, and J. Breton. 1988. Rates of primary electron transfer in photosynthetic reaction centres and their mechanistic implications. *Nature (Lond.).* 333:190–192.
14. Wasielewski, M. R., D. G. Johnson, M. S. Seibert, and Govindjee. 1989. Determination of the primary charge separation rate in isolated photosystem II reaction centers with 500 fs time resolution. *Proc. Natl. Acad. Sci. USA.* 84:1532–1536.
15. Knox, R. S., and S. Lin. 1988. Time resolution and kinetics of "F680" at low temperatures in spinach chloroplasts. *In* Photosynthetic Light-Harvesting Systems: Organization and Function. H. Scheer and S. Schneider, editors. W. de Gruyter, Berlin. 567–578.
16. Seely, G. R. 1973. Energy transfer in a model of the photosynthetic unit of the green plant. *J. Theor. Biol.* 40:189–199.
17. Gulotty, R. J., L. Mets, R. S. Alberte, and G. R. Fleming. 1985. Picosecond fluorescence study of photosynthetic mutants of *Chlamydomonas reinhardtii:* origin of the fluorescence decay of chloroplasts. *Photochem. Photobiol.* 41:487–496.
18. Hodges, M., and I. Moya. 1986. Time-resolved chlorophyll fluorescence studies of photosynthetic membranes: resolution and characterization of four kinetic components. *Biochim. Biophys. Acta.* 849:193–202.